Sensors and Actuators B 255 (2018) 638–646

Contents lists available at ScienceDirect

Sensors and Actuators B: Chemical

journal homepage: www.elsevier.com/locate/snb

# Miniaturized planar room temperature ionic liquid electrochemical gas sensor for rapid multiple gas pollutants monitoring

Hao Wan[a,*], Heyu Yin[a], Lu Lin[b], Xiangqun Zeng[b,*], Andrew J. Mason[a,*]

[a] Department of Electrical and Computer Engineering, Michigan State University, East Lansing, MI, 48824, USA
[b] Department of Chemistry, Oakland University, Rochester, MI, 48309, USA

ARTICLE INFO

*Article history:*
Received 28 April 2017
Received in revised form 4 August 2017
Accepted 12 August 2017
Available online 18 August 2017

*Keywords:*
Electrochemical gas sensor
Miniaturized sensor
Planar platinum electrode
Room temperature ionic liquid

ABSTRACT

The growing impact of airborne pollutants and explosive gases on human health and occupational safety has escalated the demand of sensors to monitor hazardous gases. This paper presents a new miniaturized planar electrochemical gas sensor for rapid measurement of multiple gaseous hazards. The gas sensor features a porous polytetrafluoroethylene substrate that enables fast gas diffusion and room temperature ionic liquid as the electrolyte. Metal sputtering was utilized for platinum electrodes fabrication to enhance adhesion between the electrodes and the substrate. Together with carefully selected electrochemical methods, the miniaturized gas sensor is capable of measuring multiple gases including oxygen, methane, ozone and sulfur dioxide that are important to human health and safety. Compared to its manually-assembled Clark-cell predecessor, this sensor provides better sensitivity, linearity and repeatability, as validated for oxygen monitoring. With solid performance, fast response and miniaturized size, this sensor is promising for deployment in wearable devices for real-time point-of-exposure gas pollutant monitoring.



## 1. Introduction

Airborne pollutants such as $O_3$ (ozone) and $SO_2$ (sulfur dioxide) are of great concerns due to their adverse and deadly impact on human health [1]. Furthermore, explosive gases and oxidizers such as $CH_4$ (methane) and $O_2$ (oxygen) need to be observed regularly for occupational safety [2]. Although a variety of gas sensors have been developed to monitor air pollutants and gaseous hazards, most existing tools are, unfortunately, incapable of accurately measuring acute exposure on site due to their intrinsic limitations in physical size, response time and/or repeatability [3]. A robust and wearable-sized gas sensor that is capable of real-time point-of-exposure monitoring could provide immediate alerts of gaseous hazards to vulnerable individuals. Furthermore, such a sensor could be widely deployed in wearable devices deployed across large areas to provide vital location- and time-tagged exposure data for human health assessment and timely treatment notices and safety alerts, as illustrated in Fig. 1.

Gas sensing technologies that have been widely studied, and popular options include metal oxide semiconductor, optical, surface acoustic wave and electrochemical [4]. Among these, electrochemical sensing offers attractive features and performance including low cost, low power consumption, high sensitivity and high selectivity [5,6], which are all very important for acute exposure monitoring applications. Furthermore, the instrumentation for electrochemical sensing has been implemented in complementary metal oxide semiconductor (CMOS) chips [7], allowing the entire sensor system to be realized in miniaturized and wearable formats. However, an inherent drawback of conventional electrochemical sensors is that their lifetime is highly limited due to evaporation of supporting liquid electrolytes [8]. To overcome this limitation, room temperature ionic liquids (RTIL) have been utilized as electrolytes in many new electrochemical gas sensors [9–11]. The low vapor pressure, electrochemical and thermal stability and high ionic conductivity of RTILs ensure a long operation lifetime and excellent performance for electrochemical gas sensors [12,13]. On the other hand, existing RTIL-based electrochemical sensors suffer from relatively large physical dimensions and/or long measurement time that limit their use in point-of-exposure monitoring of gaseous hazards [6,14]. Also, very few existing sensors demonstrate the capability to measure multiple gases, which is an important requirement in many applications including air pollutant monitoring.

This paper introduces a new, miniaturized, planar RTIL electrochemical (MPRE) gas sensor for rapid multiple gas pollutant

* Corresponding authors.
*E-mail addresses:* wh1816@msu.edu (H. Wan), zeng@oakland.edu (X. Zeng), mason@msu.edu (A.J. Mason).

http://dx.doi.org/10.1016/j.snb.2017.08.109
0925-4005/

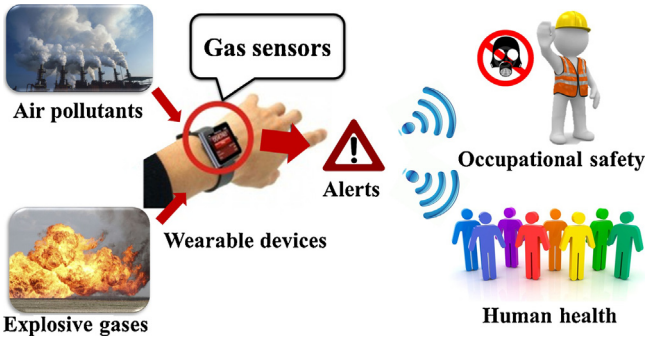


**Fig. 1.** Applications of gas sensors deployed in wearable devices for real-time point-of-exposure gas monitoring.

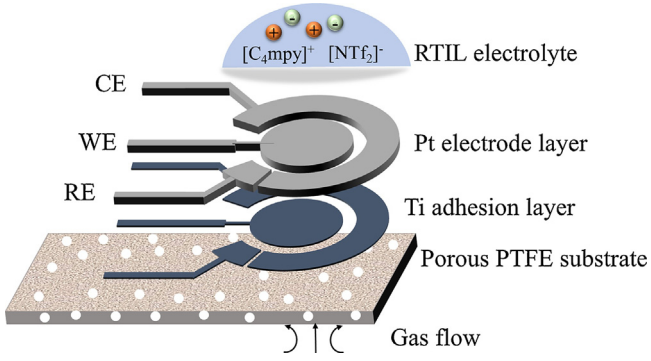


**Fig. 2.** The structure schematic of the MPRE gas sensor including porous PTFE substrate, titanium adhesion layer, platinum electrode layer and RTIL electrolyte.

monitoring. Evolving from our prior work on a miniaturized gold planar electrode gas sensors [12], the MPRE sensor utilizes platinum sensing electrodes and introduces a new fabrication process to improve the adhesion between electrodes and the substrate. Four different gases, oxygen, methane, sulfur dioxide and ozone were tested to verify the performance of the MPRE sensor.

## 2. Experimental

### 2.1. MPRE gas sensor design

A variety of RTIL-based electrochemical sensors have been developed for gas measurement. In most of these, RTIL is coated atop a set of electrodes supported on a solid substrate [15], and gases must diffuse through the RTIL electrolyte to reach the electrode surface. Because of the high viscosity of RTIL [16], this typical structure exhibits a long response time that limits its application in real-time point-of-exposure measurement.

To shorten the response time of RTIL-based gas sensors, we previously reported a macro-scale Clark cell that was manually assembled by stacking platinum mesh (working electrode), filter paper (insulator) and platinum wires (counter and reference electrodes) on top of a thin sheet of porous polytetrafluoroethylene (PTFE) [17]. The porous PTFE substrate allowed a pathway for gas to quickly reach the electrode/electrolyte interface without diffusing through RTIL, which generated a substantial improvement in response time. However, this device was produced using a manual assembly process that generated an undesirable performance variation between devices and limited miniaturization of the sensor.

To enable sensor miniaturization and reduce performance variability maintaining the rapid response of our PTFE structure, our group previously introduced a gas sensor that utilized microfabrication processes to form planar gold electrodes on a porous PTFE substrate [12]. The MPRE gas sensor presented in this paper adopts our prior porous PTFE and introduces design improvements including an additional titanium layer to promote electrode adhesion to the rough porous substrate and use of a disk-shaped working electrode for better multi-gas sensing performance. As shown in Fig. 2 sensor structure diagram, porous PTFE was used as the substrate, and a titanium adhesion layer and a platinum electrode layer were subsequently deposited on the substrate. The electrodes, including working electrode (WE), reference electrode (RE) and counter electrode (CE) were observed to be reliably attached to the rough porous PTFE surface by the titanium adhesion layer. After precise metal patterning via a lift-off photolithography process, RTIL was directly added on the surface of the electrodes as the electrolyte. Due to the porosity of the substrate, gas targets can rapidly reach to the electrode surface by passing through pores in the PTFE substrate rather than permeating through the RTIL electrolyte, enabling rapid sensor response. It is worth stressing that reactions still take place at the interface of the electrode and the RTIL electrolyte though the sensor design introduces gas through the porous PTFE substrate.

### 2.2. Sensor microfabrication and packaging

Many techniques have been employed to fabricate electrochemical sensors including microfabrication [18], screen printing [19] and inkjet printing [20]. Among these, microfabrication technologies can achieve very uniform, accurate and reproducible patterning with micro/nano-sized resolution [21]. Therefore, microfabrication technologies were chosen to realize the MPRE gas sensor design.

To implement MPRE sensor microfabrication, one challenge is that microfabrication processes are difficult to perform on porous PTFE substrates due to this material's flexibility (which makes it difficult to hold in process equipment), roughness (which makes it difficult to focus photolithography processes accurately), and surface porosity (which makes adding and removing thin films difficult). To address these challenges, in prior work [12] we affixed PTFE to a glass slide to keep the substrate rigid during fabrication, and we chose AZ4620 photoresist (PR) to form a thick layer (~10 μm) that allows thin-film metals to be reliably patterned using lift-off even on the rough and porous PTFE surface. However, this prior process utilized thermal evaporation for thin-film metal deposition, which introduced high energy metal atoms that can raise the temperature of the PTFE surface higher than 300 °C. Above 120 °C, PTFE can undergo vitrification, molecular transformation to glass [22], which introduces stress to the substrate surface and was observed to promote undesired peeling of thin-film metals. Furthermore, this heat can affect PTFE pore size on the surface that may hinder gas flow through the substrate.

To overcome the shortfalls of our prior process, magnetron sputtering was chosen for thin-film metal deposition in this work rather than thermal evaporation. Sputtering releases metal atoms through momentum exchange due to collisions rather than heating and results in less heating of the PTFE surface during deposition [23]. Additionally, the electrode material was changed from gold to platinum in this design in order to improve sensitivity to multiple gases, and deposition of a titanium adhesion layer beneath platinum was added to the microfabrication flow to further improve reliability of metal attachment to the rough PTFE substrate. Fig. 3 describes the microfabrication process used to fabricate the MPRE gas sensor. First, a glass slide was cleaned in oxygen plasma, and PTFE membrane with 4 μm average pore size (POREX PM23J) was affixed to the glass slide by a double-sided tape. Then a 10 μm layer of AZ4620 PR was spin-coated at 2100 revolutions per minute (rpm) on the PTFE surface, and the desired electrode areas were UV exposed through a photomask as shown in Fig. 3(a). After UV exposure, the glass slide was removed, and the PR on the PTFE surface was

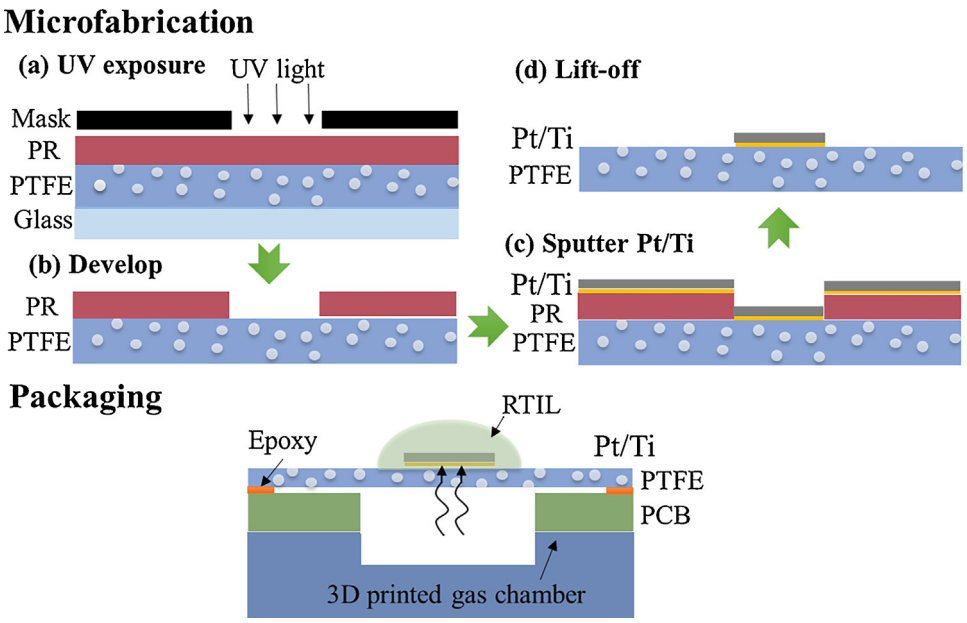


**Fig. 3.** The microfabrication process and packaging of the MPRE sensor: (a) UV exposure; (b) Develop; (c) Sputter Ti/Pt; (d) Lift-off.

developed to form the PR pattern shown in (b). Then, 5 μm titanium followed by 300 μm platinum was deposited via sputtering in (c). The thick platinum layer ensures the formation of continuous traces on the porous PTFE surface. The planar thin-film metals were then patterned via lift-off of PR in acetone overnight followed by ultrasonic cleaning for 5 min as shown in (d).

To facilitate gas flow and electrical connections during sensor characterization and use, the flexible MPRE sensors were packaged with a custom printed circuit board (PCB) and 3D-printed gas flow chamber, as shown in Fig. 3 (bottom). First, the MPRE sensor was cleaned with IPA and deionized water and then dried with nitrogen. The sensor was then attached to a PCB containing a hole drilled beneath the active WE sensing area that allows gases to diffuse to the WE from the backside. Because the sensor's porous PTFE substrate is very flexible, a small amount of resin epoxy was used to fully stretch the sensor over the hold in the PCB. Then electrodes on the substrate were connected to PCB traces using conductive silver epoxy for electrical connection to external instrumentation. The PCB assembly was then mounted on a 3D-printed flow chamber that provides interfaces to connect with different gas sources. Finally, RTIL was deposited on the surface via pipette to cover electrode areas of the MPRE sensor. Different RTIL chemical compositions can be selected to achieve selective measurements of specific gas targets [11], since gases need to be adsorbed at IL/electrode interface and/or dissolved in RTIL electrolytes that provide partial selectivity for different gases. To measure the multiple gases shown in this paper, 1-butyl-1-methylpyrrolidinium bis-(trifluoromethylsulfonyl)-imide ($[C_4mpy][NTf_2]$) (IOLITEC. Inc.) was chosen as the RTIL electrolyte. The $[C_4mpy][NTf_2]$-Pt interface on the electrode surface provides a unique catalytic property [24], which enables the MPRE sensor to measure multiple gases.

### 2.3. Electrochemical test setup

The packaged MPRE sensor was placed in a desiccator filled with calcium carbonate to minimize humidity because moisture is a known interferent in RTIL-based gas sensors [11] that must be addressed using compensation or filtering techniques prior to real-world applications. A CHI 760 (CH Instrument, USA) was utilized for oxygen and methane tests, and a VersaSTAT MC potentiostat (Princeton Applied Research, USA) was used for sulfur dioxide and ozone tests. A Gas Blender 103 (MCQ Instrument, Italy) was used for automatic gas mixing and flow control. The total gas flow rate in all tests was set to 200 standard cubic centimeters per minute (sccm) unless stated otherwise. $N_2$ was used as the background gas to mix with other gases in order to achieve air samples with different concentrations. All gases were purchased from Airgas Inc and used without further purification. Dry compressed air was used as the oxygen source, which contains about 21% oxygen.

## 3. Results and discussion

### 3.1. Electrode inspection

The MPRE gas sensor was first inspected to investigate its electrode size and surface morphology. Fig. 4(a) shows a photograph of a fabricated MPRE gas sensor after mounting on the PCB but before RTIL deposition. The overall size of the reported MPRE sensor is about $7 \times 8\,mm^2$, but the sensor geometry can be tailored to different shapes and sizes to suit application needs. The optical microscope view in Fig. 4(b) defines the structure of the three electrodes of the reported MPRE sensor; the diameter of the WE is about 1050 μm, and the width of CE and RE is about 550 μm. The gap between WE and CE is about 130 μm with a gap of 140 μm between RE and CE. Fig. 4(c) shows a close-up scanning electron microscope (SEM) image of the platinum electrode topography. Due to the porosity of the PTFE substrate, the electrode surface can also be observed to be the rough and porous, which will effectively enhance the sensing area. Fig. 4(d) provides a side view of a rough spot on the electrode using focused ion beam (FIB). The silver and black areas represent the PTFE substrate, and the grey area indicates the electrode surface. The continuous junction area with uniform color between the substrate and the electrode indicates good adhesion between the substrate and the electrode despite of the very rough surface of the substrate.

### 3.2. Oxygen sensing

Constant potential chronoamperometry is a conventional electrochemical method to evaluate the performance of gas sensors. Considering the critical role oxygen plays in human life, the MPRE

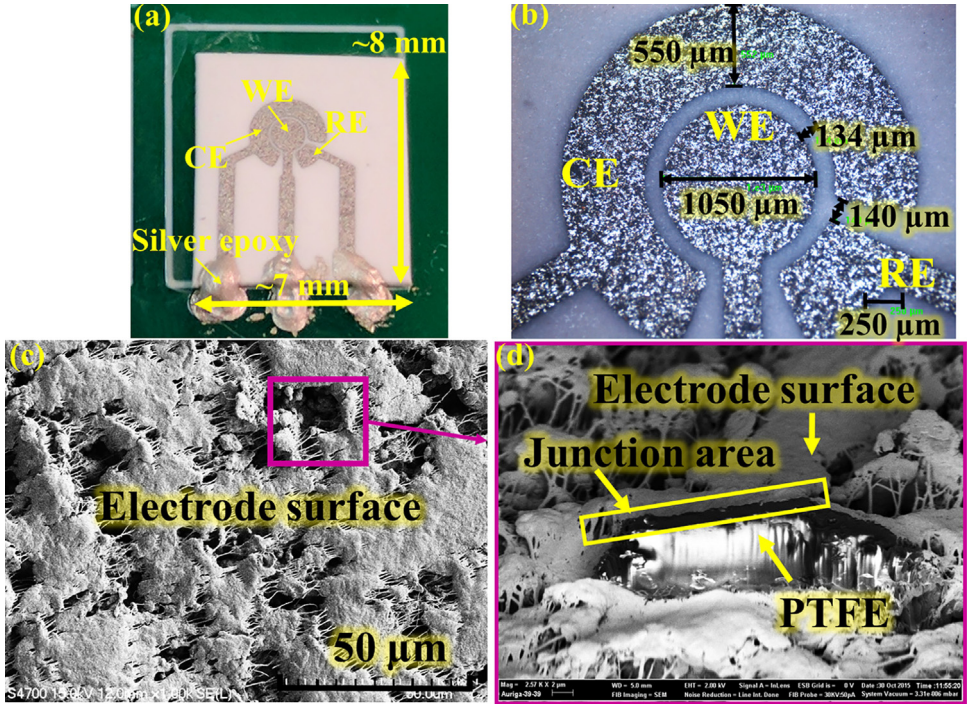


**Fig. 4.** The photo of the MPRE sensor and inspection of electrodes: (a) The photo of two packaged sensor on PCB; (b) The photo of the electrodes by optical microscope; (c) The SEM image of platinum electrode topography and (d) a side view of a rough spot on the electrode using FIB.

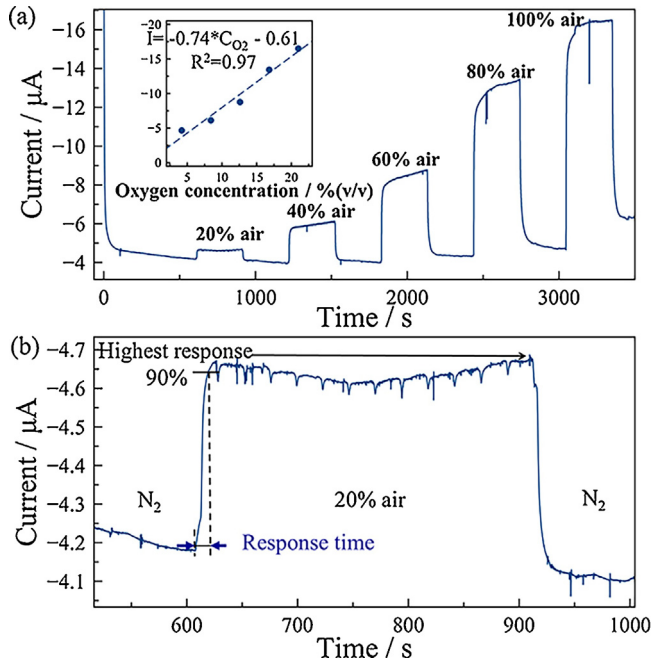


**Fig. 5.** The oxygen response of the MPRE sensor: (a) Current response for chronoamperometry at −1.2 V; (b) Calculation of response time for 20% air change. The inset of (a) shows the calibration plot of current. vs. oxygen concentration.

sensor was first tested for oxygen measurement in air samples using constant potential amperometry at −1.2 V with a sampling frequency of 50 Hz $N_2$ and different air samples were alternately pumped into the gas chamber, where the concentration of air samples was varied from 20% air to 100% air in 20% air increments. Because the air contained 21% oxygen, this effectively varied the concentration of oxygen in samples. The results in Fig. 5(a) show that the MPRE gas sensor can rapidly respond to varying oxygen concentrations, and a higher response current was recorded for higher oxygen concentrations. To characterize the sensitivity and linearity of the MPRE sensor in oxygen sensing, the highest current response in each concentration was extracted, and the plot of current vs. oxygen concentration is shown in inset of Fig. 5(a). The sensitivity of the MPRE sensor, defined as the slope of calibration equation, is 0.74 µA/[% oxygen], and the linearity is 0.97. The current change in samples with low concentration is relatively lower than that in samples with high concentration. To achieve an accurate quantification of oxygen in low concentrations, an extra calibration in low concentration range is required. Also, it was observed that the current baseline in $N_2$ period does drift, which is mainly attributed to reaction product accumulation on the electrode surface during long-term tests. To evaluate the response time of this MPRE sensor, the current response from a change of 0% air to 20% air was recorded and is plotted in Fig. 5(b). The response time, defined as the time to reach 90% of the highest current response, was measured as 10 s. This short response time can be ascribed to the porous substrate that greatly facilitates gas diffusion.

In constant potential chronoamperometry, measurements are generally conducted after sufficient decay of charging current to avoid its interference to Faradic current. However, this approach requires a long to stabilization time in practical applications, and the baseline drift always occurs due to by-products accumulation. To address these limitations, we previously introduced a new method called transient double potential amperometry for rapid gas measurements [25]. This method directly uses transient currents in the decaying stage rather than waiting for the stabilized stage to greatly shorten gas measurement time. Also, both oxidation potential and reduction potential are applied to reverse reaction products, thus eliminating the interference of by-products. To further evaluate the performance of the MPRE sensor, additional oxygen measurements were made using transient double potential amperometry. To provide a benchmark for comparison of the MPRE sensor performance, the same test methods were used with a manually-assembled Clark-cell gas sensor [17]. Both

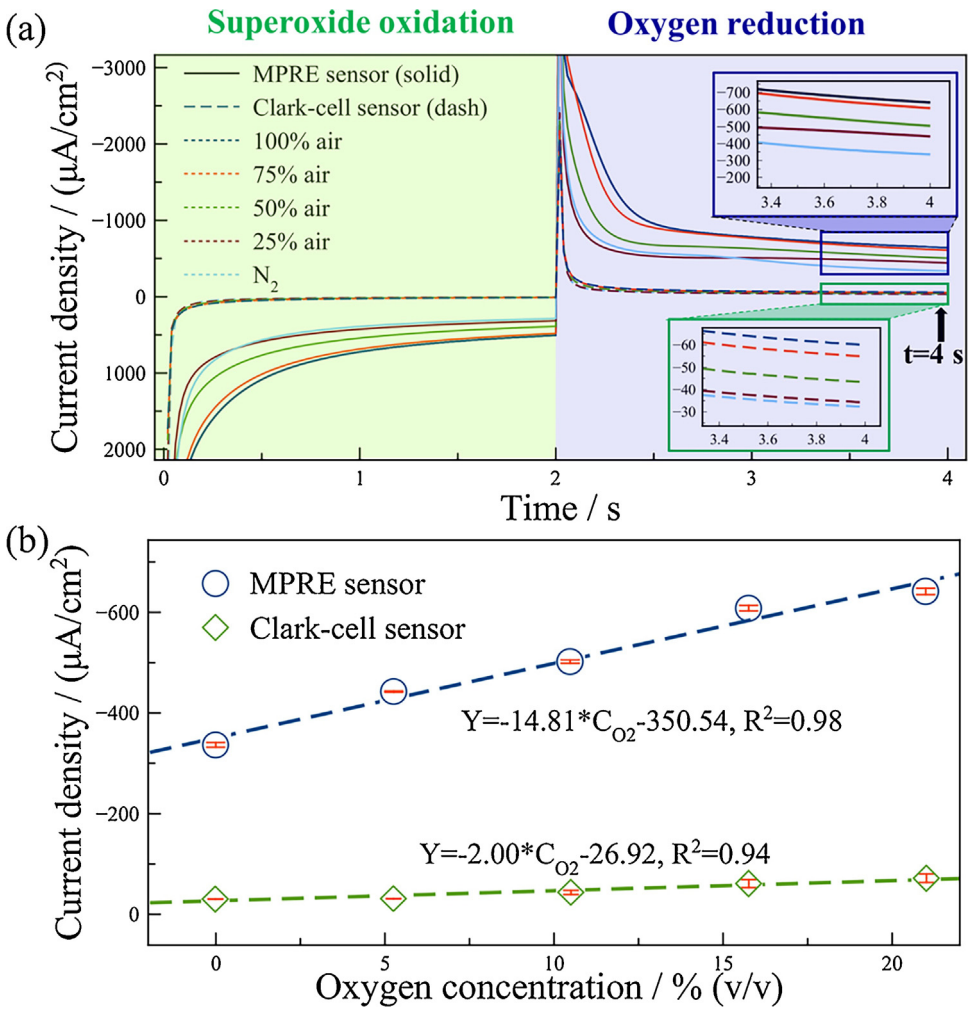


**Fig. 6.** A comparison of the MPRE sensor and Clark-cell sensor in oxygen sensing using double potential amperometry: (a) The current density response of the MPRE sensor (solid line) and Clark-cell sensor (dash line) for oxygen sensing. Both sensors were applied with 0.2 V and −1.2 V for superoxide oxidation and oxygen reduction, respectively. The inset shows the zoomed curves of Clark-cell sensor. (b) The calibration of the MPRE sensor and Clark-cell sensor for oxygen sensing. Each sample was tested for five times.

sensors were applied with an oxidation potential 0.2 V for 2 s and a reduction potential −1.2 V for 2 s. Samples 0% (100% $N_2$) to 100% air in 25% air increments were tested, and each sample was recorded five times. Considering the significant size difference of the two sensors and the linear relationship between Faradic current amplitude and sensing area according to Cottrell equation, the current density (ratio of current to sensing area) was used for direct comparison to normalize for sensing area. The sensing areas of two sensors were experimentally determined after completing all measurements, using cyclic voltammetry in 10 mM potassium ferricyanide/ferrocyanide (0.1 M KCl) according to Randles-Sevcik equation [26], and the sensing areas of the MPRE sensor and Clark-cell sensor were found to be 0.0368 $cm^2$ and 3.736 $cm^2$, respectively. After averaging results from five repetitive transient double potential amperometry tests, the averaged current density vs. time results are plotted in Fig. 6(a), which shows that two sensors present very different response curves. The current response contains a superoxide oxidation period and oxygen reduction period, and the MPRE sensor exhibits significantly higher current density in both periods compared to that of the Clark-cell sensor. The current density at 2 s into the reduction phase was extracted at each concentration and is plotted in Fig. 6(b) along with a linear calibration. The sensitivities of the MPRE sensor and Clark-cell sensor for oxygen sensing are 14.81 μA/$cm^2$/[% oxygen] and 2.00 μA/$cm^2$/[% oxygen] with a linearity of 0.98 and 0.94, respectively. The MPRE sensor demonstrated a remarkably improved sensitivity in oxygen sensing compared to that of the Clark-cell sensor. The error bar of five repetitive tests in each concentration is also plotted to characterize the repeatability of the sensors. The largest relative standard deviation (RSD) of 1.35% (0.31% oxygen) for the MPRE sensor was observed in $N_2$ (0% oxygen), and the largest for the Clark-cell sensor was 13.21% (4.08% oxygen) observed in 75% air. At all five concentrations, the RSD of the MPRE sensor is much smaller than that of the Clark-cell sensor, denoting better repeatability of the MPRE sensor in oxygen sensing. It is worth noting that platinum acted as a quasi-reference in the MPRE sensor, and cyclic voltammetry was used to track the reference potential drift during oxygen measurement. The potential drifted about 90 mV negatively in 21% oxygen compared with the oxygen reduction potential in 5.25% oxygen. Since constant potential chronoamperometry was used in our measurements, the potential drift was not taken into account to simplify all experiments.

### 3.3. Oxygen-methane coupling test

Methane is one of the major greenhouse gases that cause global climate warming. Moreover, methane is important in the mining industry due to its explosive and flammable nature that causes

occupational safety hazards. To address these potential threats, a methane sensor enabling real-time point of exposure monitoring is of great importance and necessitates investigation. Due to the kinetically low electrooxidation rate of methane, a methane-oxygen coupling reaction in [$C_4$mpy][$NTf_2$] was introduced to promote the reaction at room temperature [24,27], and the total reaction mechanism is described by:

$$CH_4 + 2O_2 \rightarrow CO_2 + 2H_2O \quad (1)$$

$$2CH_4 + 3O_2 \rightarrow 2CO + 4H_2O \quad (2)$$

where methane can be oxidized to carbon dioxide ($CO_2$) and carbon monoxide (CO) depending on the oxygen concentration during methane oxidation. This coupling reaction was utilized on the MPRE sensor to study its performance in methane sensing.

In this study, the potentials for oxygen reduction and methane reduction were set −1.2 V and 0.9 V, respectively. The period for reduction and oxidation were set to 10 s each. By adjusting flow rates of 100% air and 10% methane, six samples of different methane concentration were tested, and each concentration was tested five times using double potential chronoamperometry. Each gas sample was continuously pumped for 30 min before measurement to maintain a stable gas environment.

After averaging the five repetitive results, the currents recorded from five repetitive tests were averaged and are plotted vs. time in Fig. 7(a) for six methane concentrations. In both the oxygen reduction phase and methane oxidation phase, the current amplitude was observed to decrease over time, mainly due to the decay of charging current. The MPRE sensor presents different current response to different gas samples. Similar to the method employed for oxygen sensing, the currents at 10 s (end point of reduction phase) and 20 s (end point of oxidation phase), shown in insets of Fig. 7(a), were extracted for further sensor calibration. The calibration curve in Fig. 7(b) shows that the MPRE sensor reduction-phase current magnitudes exhibit a positive linear relationship to oxygen concentration, with a sensitivity of 0.22 μA/[% oxygen] and a linearity of 0.96 for oxygen sensing. Based on the measured sensitivity and largest standard deviation, the MPRE sensor presents a resolution of 0.60% oxygen in oxygen-methane coupling test. Also, small error bars obtained from five repetitive tests indicate good repeatability of the MPRE sensor in oxygen sensing with a largest RSD of 1.2%. A relatively low current change is also observed in samples with low concentrations, indicating a relatively low sensitivity. Thus, an accurate calibration is also required in cases that the sensor is used in samples with low oxygen concentration.

The calibration curve in Fig. 7(c) shows that the MPRE sensor oxidation-phase currents exhibit a positive linear relationship to methane concentration, up to at least 6% methane, with a sensitivity of 0.31 μA/[% methane] and a linearity of 0.9991 for methane sensing. Somewhere between 6% and 8% methane, the current amplitude was observed to start decreasing with higher methane concentrations. This phenomenon is believed to be attributed to the incomplete oxidation of methane at high concentrations. Excess methane could lower the current response due to insufficient supply of oxygen for oxidation. According to Eqs. (1) and (2), the mole ratio of oxygen to methane should be larger than 1.5 to guarantee that all methane is consumed during oxidation. At standard temperature and pressure, this correlates to a critical oxygen-to-methane volume ratio of 1.38. Notice that the fourth sample with 6% methane, has a volume ratio of 1.4, just larger than the critical ratio, and methane appears to be fully oxidized by oxygen. However, the ratio of the fifth sample with 8% methane is only 0.525, far smaller than the critical ratio, denoting insufficient consumption of methane. Thus, the red zone in Fig. 7(c) indicates where methane could not be fully oxidized and the methane concentration is out of range for the MPRE sensor. Based on the measured sensitivity and largest standard deviation, the resolution for methane sensing is 0.28% methane in this oxygen-methane coupling test. The RSD in all samples is below 1%, showing very good repeatability of the MPRE sensor for methane measurement.

### 3.4. Sulfur dioxide sensing

To validate the MPRE sensor's capability for point-of-exposure multi-gas monitoring beyond oxygen and methane, air pollutants including sulfur dioxide ($SO_2$) and ozone ($O_3$) were also tested. To implement electrochemical measurement of $SO_2$, the mechanism of $SO_2$ electroreduction in RTIL is [28,29]:

$$SO_2 + e^- \leftrightarrows SO_2^- \quad (3)$$

where sulfur dioxide can be reduced to the $SO_2^-$ radical at a certain negative potential. For each test sample, the sensor was first biased at 0 V for 10 min for conditioning and then a negative potential of −1.5 V was applied for 10 s to measure sulfur dioxide reduction current. Six samples with concentrations varying from 0 ppm (part per million in volume) to 2500 ppm were tested by setting the flow rate of nitrogen to 100 sccm and varying the flow rate of a 5000 ppm $SO_2$ source from 0 sscm to 100 sccm with 20 sccm increments. The current response of the MPRE sensor for different samples is shown in Fig. 8(a). These curves present a decaying current response with current magnitude increasing with higher $SO_2$ concentrations. Currents at both 3 s and 10 s were extracted for calibration and are plotted in Fig. 8(b). The sensitivity of the MPRE sensor for $SO_2$ measurement is 0.13 μA/100 ppm and 0.18 μA/100 ppm at 3 s and 10 s with a linearity of 0.92 and 0.97, respectively. Thus, higher sensitivity and linearity were observed with longer reduction times. The tests for 2222 ppm $SO_2$ were repeated five times as shown in Fig. 8(c), and the MPRE sensor presents a resolution of 209 ppm for $SO_2$ sensing based on the largest variation. The RSD in the repetitive tests is 0.91%, denoting very good repeatability of the sensor in $SO_2$ measurement.

### 3.5. Ozone sensing

Ozone is another pollutant that widely exists in air and can threaten human health. M. Carter et al. reported an amperometric gas sensor for ozone measurement using ionic liquids as the electrolyte [30]. To verify the capability of the MPRE sensor for different gases sensing, electrochemical tests were conducted using the MPRE sensor for $O_3$ measurement.

After conditioning at 0 V for 10 min, −0.8 V was applied to the sensor for 10 s for ozone reduction. Six different gas samples were tested with concentration increasing from 0 ppm to 1000 ppm in 200 ppm increments. As shown in Fig. 9(a), typical decaying current responses were obtained with current amplitude increasing with $O_3$ concentrations. Currents at 3 s and 10 s were extracted and are plotted in Fig. 9(b). For ozone measurement, the sensor exhibited a sensitivity of 0.11 μA/100 ppm and 0.064 μA/100 ppm with linearity of 0.916 and 0.921 at 3 s and 10 s, respectively. The sensitivity decreases with longer reduction time, while the linearity increases slightly. Five repetitive tests were conducted for 800 ppm $O_3$ as shown in Fig. 9(c), and the MPRE sensor presents a resolution of 92 ppm in ozone sensing based on the largest variation. The RSD in the tests is 1.85%, exhibiting good repeatability of the MPRE sensor for $O_3$ measurement.

### 3.6. Comparison

Table 1 shows a comparison of the results of this study with other work. The MPRE sensor demonstrated capability for multi-gas sensing, while most other work show only single gas measurement. Moreover, the MPRE sensor exhibits very short response time due

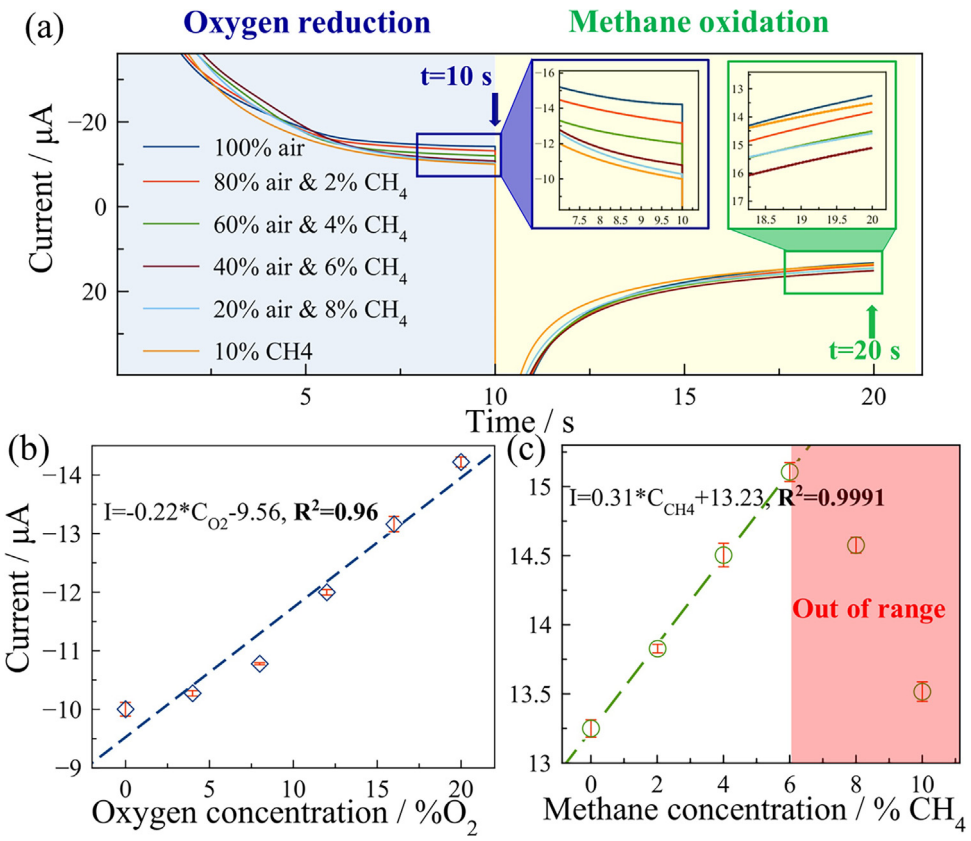


**Fig. 7.** The methane-oxygen coupling test: (a) The current response of the MPRE sensor in the coupling tests. −1.2 V was applied for oxygen reduction, and 0.9 V was applied for methane oxidation; (b)The calibration of the sensor for oxygen measurement; (c) The calibration for methane measurement, in which red zone indicates methane out of range. (For interpretation of the references to colour in this figure legend, the reader is referred to the web version of this article.)

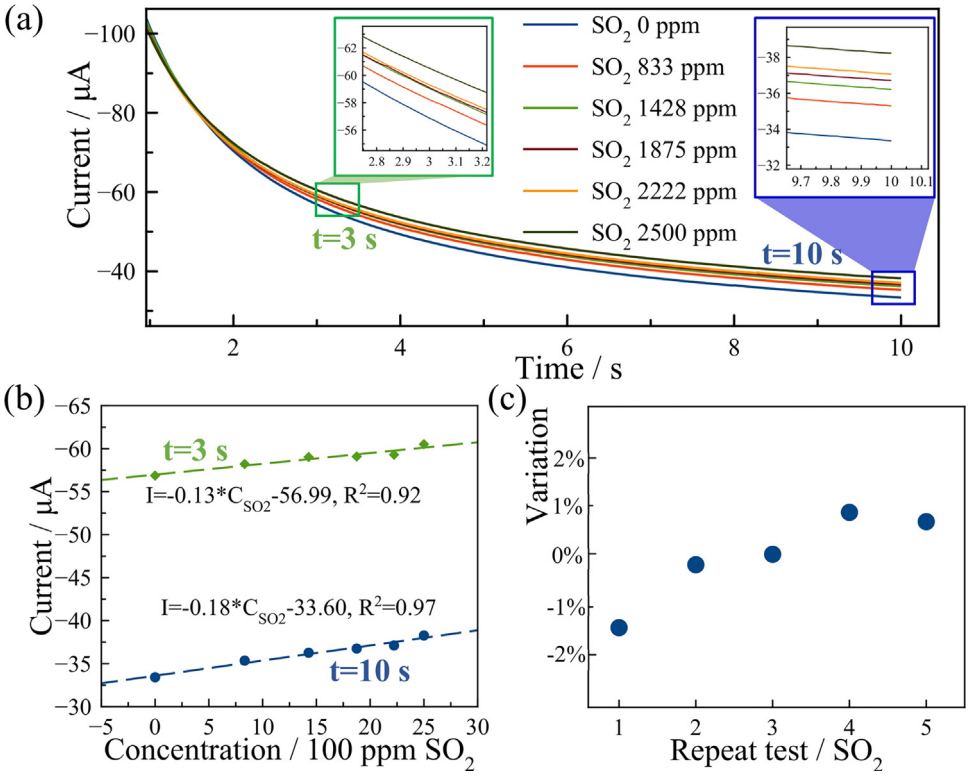


**Fig. 8.** Sulfur dioxide measurement: (a) The current response of the MPRE sensor in $SO_2$ measurement; (b) The calibration of the sensor using currents at 3 s (green) and 10 s (blue); (c) The relative variation of five repeat tests using currents at 10 s in 2222 ppm $SO_2$. (For interpretation of the references to colour in this figure legend, the reader is referred to the web version of this article.)

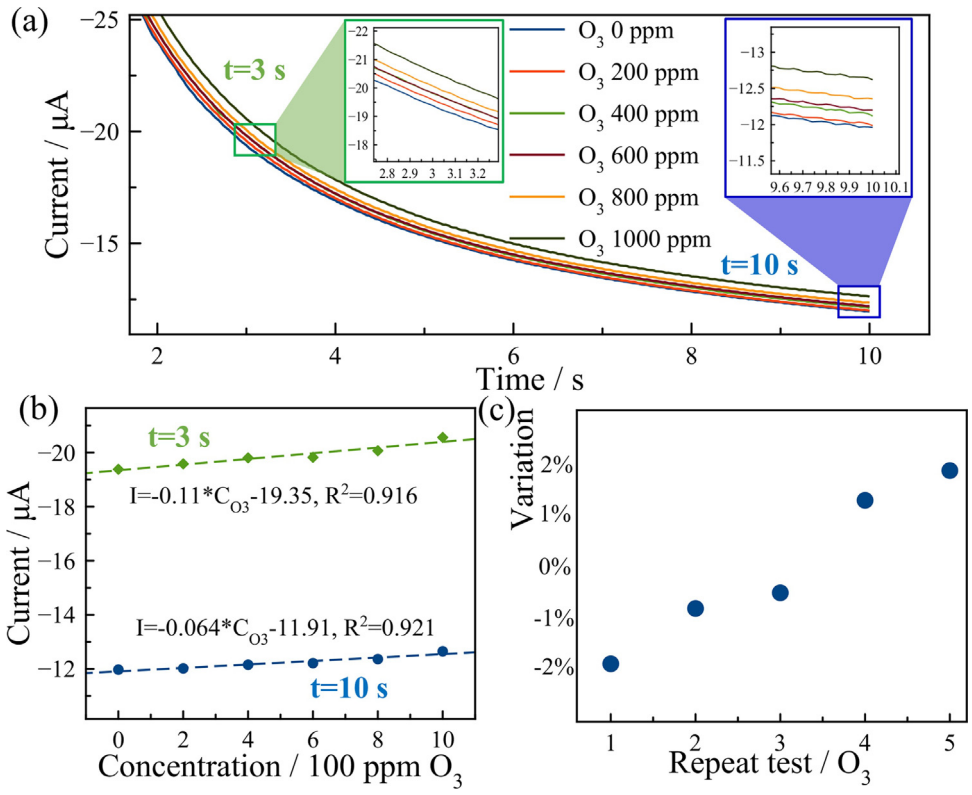


**Fig. 9.** Ozone measurement: (a) The current response of the MPRE sensor in $O_3$ measurement. (b) The calibration of the sensor using currents at 5 s (green) and 10 s (blue); (c) The relative variation of five repeat tests in 800 ppm $O_3$. (For interpretation of the references to colour in this figure legend, the reader is referred to the web version of this article.)

**Table 1**
Comparison with other work.

| | Gas Targets | Gas Diffusion | Size | Response Time |
|---|---|---|---|---|
| This work | $O_2$, $CH_4$, $SO_2$, $O_3$ | Through porous PTFE | Disk WE: diameter 1.05 mm | ~10 s |
| [13] | $O_2$ | Through thin RTIL film | Microelectrode array:~4 mm*4 mm | ~26 s |
| [15] | $O_2$ | Through porous polyethylene | Disk WE: diameter 1 mm | ~20 s |
| [27] | $O_2$ | Through thin RTIL film | Disk WE: diameter 4 mm | ~3.5 min |

to fabrication with porous PTFE that allows gas to quickly diffuse to the electrode for reaction in the thin RTIL film. Compared with other gas sensors, the MPRE is very promising in real-time point-of-exposure monitoring, and its miniaturized size facilitates the integration with wearable devices.

## 4. Conclusion

This paper introduced a new miniaturized planar RTIL electrochemical gas sensor for rapid multiple gas pollutant monitoring. A detailed fabrication process for the MPRE sensor was described to achieve good reliability. Test results show that the sensor has good sensitivity, linearity and repeatability for oxygen measurement. Additionally, methane sensing was demonstrated with a sensitivity of 0.31 μA/[% methane] and a linearity of 0.9991 in the range of 0% to 6% methane using a methane-oxygen electrochemical coupling method. $SO_2$ and $O_3$ measurements also validate the capability of the MPRE sensor for monitoring other air pollutants. These results encourage the future development of a sensor array that can simultaneously measure multiple gases in a mixed gas environment. Selectivity can be achieved by judicious choice of electrode materials, RTIL chemical composition and electrochemical method (particularly bias voltage) with data processing algorithms that have been widely applied in electronic nose systems [31]. Several algorithms have been studied in our group to achieve identification and quantification of mixed gases based on data from a gas sensor array [32,33]. Furthermore, a high sensitivity multi-channel CMOS circuit has already been developed in our group for air quality monitoring based on an RTIL-based gas sensor array [34]. Thus, the MPRE gas sensor, together with the CMOS circuit provides a very promising platform toward a miniaturized, inexpensive, rapid-response, low power, multi-gas sensing array for point-of-exposure monitoring of gaseous hazards.

## Acknowledgments

The work was supported by National Institutes of Health under NIEHS grant R01ES022302. The authors would like to thank Min Guo and Yongan Tang for helpful discussions on measuring sensor performance. Microfabrication was completed at the University of Michigan Laurie Nanofabrication Facility and the Keck Microfabrication Facility in Michigan State University.

## References

[1] M. Kampa, E. Castanas, Human health effects of air pollution, Environ. Pollut. 151 (2008) 362–367.
[2] C. Massie, G. Stewart, G. McGregor, J.R. Gilchrist, Design of a portable optical sensor for methane gas detection, Sens. Actuators B Chem. 113 (2006) 830–836.

[3] X. Liu, S. Cheng, H. Liu, S. Hu, D. Zhang, H. Ning, A survey on gas sensing technology, Sensors 12 (2012) 9635–9665.
[4] Z. Yunusa, M.N. Hamidon, A. Kaiser, Z. Awang, Gas sensors: a review, Sens. Transducers 168 (2014) 61–75.
[5] E.M. Hetrick, M.H. Schoenfisch, Analytical chemistry of nitric oxide, Annu. Rev. Anal. Chem. 2 (2009) 409–433.
[6] Z. Wang, P. Lin, G.A. Baker, J. Stetter, X. Zeng, Ionic liquids as electrolytes for the development of a robust amperometric oxygen sensor, Anal. Chem. (2011) 7066–7073.
[7] Y. Huang, A.J. Mason, Lab-on-CMOS integration of microfluidics and electrochemical sensors, Lab Chip 13 (2013) 3929–3934.
[8] N. Dossi, R. Toniolo, A. Pizzariello, E. Carrilho, E. Piccin, S. Battiston, G. Bontempelli, An electrochemical gas sensor based on paper supported room temperature ionic liquids, Lab Chip 12 (2012) 153–158.
[9] M.C. Buzzeo, C. Hardacre, R.G. Compton, Use of room temperature ionic liquids in gas sensor design, Anal. Chem. 76 (2004) 4583–4588.
[10] D. Wei, A. Ivaska, Applications of ionic liquids in electrochemical sensors, Anal. Chim. Acta 607 (2008) 126–135.
[11] D.S. Silvester, Recent advances in the use of ionic liquids for electrochemical sensing, Analyst 136 (2011) 4871.
[12] X. Mu, Z. Wang, X. Zeng, A.J. Mason, A robust flexible electrochemical gas sensor using room temperature ionic liquid, IEEE Sens. J. 13 (2013) 3976–3981.
[13] X.J. Huang, L. Aldous, A.M. Omahony, F.J. Del Campo, R.G. Compton, Toward membrane-free amperometric gas sensors: a microelectrode array approach, Anal. Chem. 82 (2010) 5238–5245.
[14] J. Lee, D.S. Silvester, Low-cost microarray thin-film electrodes with ionic liquid gel-polymer electrolytes for miniaturised oxygen sensing, Analyst (2016) 3705–3713.
[15] W. Rong, O. Takeyoshi, K. Fusao, O. Takeo, A novel amperometric $O_2$ gas sensor based on supported room- temperature ionic liquid porous polyethylene membrane-coated electrodes, Electroanalysis 16 (2004) 66–72.
[16] S. Pandey, Analytical applications of room-temperature ionic liquids: a review of recent efforts, Anal. Chim. Acta. 556 (2006) 38–45.
[17] Z. Wang, X. Mu, M. Guo, Y. Huang, A.J. Mason, X. Zeng, Methane recognition and quantification by differential capacitance at the hydrophobic ionic liquid-electrified metal electrode interface, J. Electrochem. Soc. 160 (2013) B83–B89.
[18] M. Toner, H. Buettner, Microfabrication in biology and medicine, Biotechnol. Prog. 14 (1998), 355–355.
[19] K. Murugappan, J. Lee, D.S. Silvester, Comparative study of screen printed electrodes for ammonia gas sensing in ionic liquids, Electrochem. Commun. 13 (2011) 1435–1438.
[20] M. Singh, H.M. Haverinen, P. Dhagat, G.E. Jabbour, Inkjet printing-process and its applications, Adv. Mater. 22 (2010) 673–685.
[21] G.C. Fiaccabrino, M. Koudelka-Hep, Thin-film microfabrication of electrochemical transducers, Electroanalysis 10 (1998) 217–222.
[22] I. Tzanakis, M. Conte, M. Hadfield, T.A. Stolarski, Experimental and analytical thermal study of PTFE composite sliding against high carbon steel as a function of the surface roughness, sliding velocity and applied load, Wear 303 (2013) 154–168.
[23] P.J. Kelly, R.D. Arnell, Magnetron sputtering: a review of recent developments and applications, Vacuum 56 (2000) 159–172.
[24] Z. Wang, X. Zeng, Bis(trifluoromethylsulfonyl)imide ($NTf_2$)-based ionic liquids for facile methane electro-oxidation on Pt, J. Electrochem. Soc. 160 (2013) H604–H611.
[25] H. Wan, H. Yin, A.J. Mason, Rapid measurement of room temperature ionic liquid electrochemical gas sensor using transient double potential amperometry, Sens. Actuators B Chem. 242 (2017) 658–666.
[26] I. Taurino, S. Carrara, M. Giorcelli, A. Tagliaferro, G. De Micheli, Comparison of two different carbon nanotube-based surfaces with respect to potassium ferricyanide electrochemistry, Surf. Sci. 606 (2012) 156–160.
[27] Z. Wang, M. Guo, G. a Baker, J.R. Stetter, L. Lin, A.J. Mason, X. Zeng, Methane-oxygen electrochemical coupling in an ionic liquid: a robust sensor for simultaneous quantification, Analyst 139 (2014) 5140–5147.
[28] L.E. Barrosse-Antle, D.S. Silvester, L. Aldous, C. Hardacre, R.G. Compton, Electroreduction of sulfur dioxide in some room-temperature ionic liquids, J. Phys. Chem. C 112 (2008) 3398–3404.
[29] E. Potteau, E. Levillain, J.P. Lelieur, Mechanism of the electrochemical reduction of sulfur dioxide in non-aqueous solvents, J. Electroanal. Chem. 476 (1999) 15–25.
[30] M.T. Carter, J.R. Stetter, M.W. Findlay, V. Patel, Amperometric gas sensors with ionic liquid electrolytes, ECS Trans. 58 (2014) 7–18.
[31] S.M. Scott, D. James, Z. Ali, Data analysis for electronic nose systems, Microchim. Acta 156 (2006) 183–207.
[32] Yuning Yang, A.J. Mason, Identification and quantification of mixed air pollutants based on homotopy method for gas sensor array, IEEE Eng. Med. Biol. Soc. (2012) 4221–4224.
[33] Y. Yang, J. Yi, R. Jin, A.J. Mason, Power-error analysis of sensor array regression algorithms for gas mixture quantification in low-power microsystems, IEEE Sens. (2013) 1–4.
[34] H. Li, C.S. Boling, A.J. Mason, CMOS amperometric ADC with high sensitivity, dynamic range and power efficiency for air quality monitoring, IEEE Trans. Biomed. Syst. 10 (2016) 1–11.

## Biographies

**Hao Wan** received the B.S. and Ph.D. degree in Biomedical Engineering from Huazhong University of Science and Technology, Wuhan, China and Zhejiang University, Hangzhou, China in 2010 and 2015, respectively. He is currently a postdoc in the Department of Electrical and Computer Engineering, Michigan State University, East Lansing, MI, USA. His research interests are sensor microfabrication, electrochemical sensing and instrument development in environmental monitoring applications.

**Heyu Yin** revived the B.S. degree in Engineering management from Hubei University, Wuhan, China and Master degree in Microelectronics and Nanoelectronics from Tsinghua University, Beijing, China. He is currently a Ph.D. student in the Department of Electrical and Computer Engineering, Michigan State University, East Lansing, MI, USA. His research interests are electrochemical sensor and lab-on-CMOS integration for portable biosensing and environmental monitoring application.

**Lu Lin** received the B.S. degree in Applied Chemistry from Shanghai University (Shanghai, China) in 2004 M.S. degree in Chemistry from University of Detroit Mercy (Detroit, Michigan, USA) in 2011. He is currently perusing Ph.D. degree in Chemistry at Oakland University (Rochester, Michigan, USA). His research interests are analytical method development, characterization and validation of ionic liquid electrochemical gas sensors for multiple gas detection.

**Xiangqun Zeng** is a professor of Chemistry at Oakland University, Rochester, MI. She obtained her Ph.D. in electrochemistry and surface chemistry from SUNY at Buffalo with Stanley Bruckenstein in 1997. Her lab focuses on the fundamental and applied research of ionic liquids and conductive polymers at solid electrodes, development of new analytical techniques, chemical and biosensors.

**Andrew J. Mason** received the B.S. degree in physics with highest distinction from Western Kentucky University, Bowling Green, KY, USA, in 1991, the BSEE (honors) from the Georgia Institute of Technology, Atlanta, GA, USA, in 1992, and the M.S. and Ph.D. degrees in electrical engineering from the University of Michigan, Ann Arbor, MI, USA, in 1994 and 2000, respectively. Hi is currently a full professor in the Department of Electrical and Computer Engineering, Michigan State University, East Lansing, MI, USA. His research explores mixed-signal circuits, microfabricated structures, and machine learning algorithms for integrated microsystems in biomedical, environmental monitoring, and sustainable lifestyle applications.